

G. V. Gibbs · D. F. Cox · M.B. Boisen, Jr.  
R. T. Downs · N. L. Ross

## The electron localization function: a tool for locating favorable proton docking sites in the silica polymorphs

Received: 9 September 2002 / Accepted: 14 February 2003

**Abstract** The ELF electron localization function was used to locate regions ascribed to localized nonbonding electrons as favorable docking sites for hydrogen atoms in coesite, quartz, and stishovite. A mapping of the function for a series of representative hydroxyacid disilicate and cyclosiloxane molecules indicates that the nonbonding regions on the bridging oxide anions involved in narrow SiOSi angles are more favorable as docking sites than those involved in wide angles. It also indicates that the nonbonding regions associated with the nonbridging oxide anions comprising surface SiOH dangling bonded interactions are likewise favorable docking sites. ELF descriptions of the nonbonding and bonding regions for coesite and quartz were found to be similar to those obtained for the molecules. For a protonated coesite crystal, the function was also used to deduce the positions of the model H atoms of a defect  $v(\text{OH})_4$  group where  $v$  is the vacancy left by Si. The positions of the H atoms were found to be in reasonable agreement with those determined in an infrared study, particularly for those bonded to anions involved in narrow SiOSi angles. A mapping of the ELF indicates that the OH vector reported for stishovite is oriented nearly perpendicular ( $92.5^\circ$ ) to [001], as found in infrared studies. The nonbonding region displayed by the function was used to locate the position

of the H atom at a distance of  $0.96 \text{ \AA}$  from the non-equivalent oxide anion comprising the shared edge of the silicate octahedra. The positions of model hydrogen atoms comprising a potential defect  $v(\text{OH})_4$  group in quartz were also deduced on the basis of the positions of the local maxima of the nonbonding regions. When used in conjunction with spectroscopic methods, the strategy used in this study should be useful in locating protons in Earth materials with trace amounts of H. Maxima ascribed to regions of bonding and nonbonding electrons displayed in the ELF maps were found to be in close correspondence with those displayed in valence, deformation, and Laplacian electron-density distributions. Collectively, these results indicate that the electron density is localized in the nonbonded regions of the anions involved in the narrow SiOSi angles (angles less than  $\sim 150^\circ$ ) in silica polymorphs like quartz and coesite and much less so for the anions involved in wider angles.

### Introduction

The ELF electron localization function is a dimensionless, empirical function in 3-space that generates relatively large values ranging between 0.5 and 1.0 in regions that can be ascribed to bonding and nonbonding localized electrons and smaller values (less than 0.5) where one expects the electrons to be delocalized (Bader et al. 1996; Burdett and McCormick 1998). Since its definition by Becke and Edgecombe (1990), workers have found the function to be a useful tool for studying bonded interactions, particularly given that the positions of the bonding and nonbonding regions of localized electrons tend to conform with the classic picture of chemical bonding as embodied in the Lewis (1966) and Gillespie (1970) models of molecular geometry. Among other things, the function has been used (1) to characterize the bonded interactions for a variety of materials ranging from insulators to metals, (2) to elucidate the structural properties of water in the dissociation of the  $\text{H}_2\text{O}$

G. V. Gibbs (✉) · N. L. Ross  
Department of Geological Sciences,  
Virginia Tech., Blacksburg, Virginia 24061-0420, USA  
E-mail: ggibbs@vt.edu

D. F. Cox  
Department of Chemical Engineering,  
Virginia Tech., Blacksburg, Virginia 24061-0420, USA

M.B. Boisen, Jr.  
Department of Mathematics,  
University of Idaho, Idaho 83844, USA

R. T. Downs  
The Department of Geosciences,  
University of Arizona, Tucson, Arizona 85721, USA

*Present address:* G. V. Gibbs, in care of M. Spackman  
Department of Chemistry, University of New England,  
Armidale 2351, Australia

molecule into  $\text{OH}^-$  and  $\text{H}_3\text{O}^+$  ions, (3) to provide evidence that the semimetallic interactions in selected chalcogenides arise from “lone-pair–lone-pair interactions” and (4) to establish a connection between the docking of the protons in the high-pressure silica polymorph coesite and the oxides anions in the structure that exhibit nonbonding regions (cf. Savin et al. 1997; Trout and Parrinello 1999; Fuster and Silvi 2000; Gibbs et al. 2001, 2002; Raulot et al. 2002).

### Proposed study

In an analysis of the polarized Fourier transform infrared (FTIR) absorption spectra recorded for several protonated coesite crystals synthesized at high pressures and temperatures, Koch–Müller et al. (2001) concluded that hydrogen is bonded to four of the five nonequivalent oxide anions forming a defect  $\nu(\text{OH})_4$  group where  $\nu$  is the vacancy created by a missing Si atom (see also Mosenfelder 2000). An examination of the crystal structure revealed that the four anions (O2, O3, O4, and O5) comprising the group involve SiOSi angles less than  $\sim 150^\circ$ . No H atoms were found to be bonded to the remaining O1 anion that involves the wide  $180^\circ$  angle. The observation that the oxide anions comprising the group are all involved in relatively narrow angles suggests that a connection exists between the angle and the extent to which the nonbonding region of localized electrons on an anion is developed (Gibbs et al. 2002).

In this study, we will explore the connection between the SiOSi angle and the nonbonding regions and their favorability as proton-docking sites in the silica polymorphs and related representative molecules. We will also present a strategy for locating the positions of the protons. Three features of the ELF isosurfaces associated with a nonbonding region, referred to as the ELF description, will be considered: (1) the value of the ELF at the local maximum of the nonbonding region, (2) the position of the maximum, and (3) the shape of the ELF isosurface at a given percentile near the local maximum. The ELF description of the nonbonding regions will be used to determine whether the regions in coesite correspond with the proton docking sites determined by Koch–Müller et al. (2001). In addition, the positions of the protons in coesite, quartz, and stishovite will be deduced based on the positions of the oxide anions and the local maxima of the associated nonbonding regions. As the ELF is an empirical and dimensionless function, it is important to note that there is no clear-cut way of connecting the value of the function at a given point to the value of the electron density at that point. Nonetheless, we will show that the isosurfaces and maxima in the bonding and nonbonding regions displayed by valence ( $\rho$ ), deformation ( $\Delta\rho$ ), and Laplacian ( $-\nabla^2\rho$ ) electron density maps correspond with those displayed by the ELF maps. In other words, the correspondence will show that there exists an one-to-one relationship in the majority of cases between the isosurfaces and the

maxima of the ELF maps and those displayed by  $\rho$ -,  $\Delta\rho$  and  $-\nabla^2\rho$  maps (see also Bader et al. 1996).

---

## Molecular and crystal model structures and computations

### Model structures

As the bridging SiO bond length and SiOSi angle variations generated for the hydroxyacid acid disilicate  $\text{H}_6\text{Si}_2\text{O}_7$  molecule are strikingly similar to those observed for quartz and coesite (Gibbs 1982; Gibbs et al. 2001), the molecule has found use as a representative model for studying the bonded interactions of the silica polymorphs and related materials and the docking of water molecules on a model silica surface (Gibbs 1982; Lasaga and Gibbs 1990; Lasaga 1990). Also, an ELF map generated for the molecule for an ELF value of 0.844 shows that the isosurfaces that envelop the local maxima are teardrop-shaped in the bonding regions and banana-shaped in the nonbonding regions for the SiOSi bonded interactions. These features are virtually identical with those displayed for quartz generated with the same ELF value (Gibbs et al. 2002). Given this close correspondence, the molecule will be used to explore the degree to which the ELF description of the nonbonding regions depends on the SiOSi angle. For the study, an ELF description will be undertaken for several hydroxyacid disilicate molecules. To obtain a clear picture of how the ELF is distributed near a local maximum, we will generate isosurfaces that correspond to ELF values set at 98% of the local maximum value. This 98th percentile view will provide a picture of the localization function isosurface in the nonbonding region and the value of the local maximum will provide a measure of the extent to which the function is developed in the region. As a matter of convenience, the position of the local maximum will be taken as the position of the nonbonding region.

In the calculations, the SiOSi angle of the disiloxane anion of the  $\text{H}_6\text{Si}_2\text{O}_7$  molecule was clamped at a range of values and ELF isosurface maps were generated for each resulting structure. As the  $(\text{H}_2\text{SiO})_n$ -cyclosiloxane molecules exhibit a similar range of bond lengths and angles, calculations were completed for these molecules as well, given that silicate rings are common structural units in the silica polymorphs and related framework silicates. It will be of interest to explore the extent to which the nonbonding ELF description depends on the size of the ring and the associated SiOSi angle. It will likewise be of interest to see whether the nonbonding regions are reducible and have two distinct maxima or have one and are irreducible.

### Computations

The geometries of the  $\text{H}_6\text{Si}_2\text{O}_7$  and  $(\text{H}_2\text{SiO})_n$  ( $n = 2, 3, \dots, 8$ ) molecules were each optimized at the

Becke3LYP 6-311G(2d,p) level using the GAUSSIAN98 software. In the case of the  $\text{H}_6\text{Si}_2\text{O}_7$  molecules, the silicate tetrahedra of the molecules were oriented in a staggered configuration to match that observed for the tetrahedra in quartz, cristobalite, and several of those in coesite. In addition,  $C_v$  point group symmetry was assumed and the geometries of the molecules were optimized with the SiOSi angle clamped at  $10^\circ$  intervals between and including  $110^\circ$  and  $180^\circ$ . In addition, the geometry of the molecule was optimized for both a singly and doubly eclipsed arrangement of silicate tetrahedra for the same set of SiOSi angles, but since the ELF descriptions for the nonbonding regions for these molecules are not appreciably different from those of the staggered structure, they will not be discussed here. The geometry of each molecule was constrained with  $C_v$  point symmetry to prevent the H atoms on the non-bridging oxide anions from bonding with the bridging and the other nonbridging oxide anions. The geometry of each  $(\text{H}_2\text{SiO})_n$ -cyclosiloxane molecule was optimized assuming  $D_{nh}$  point symmetry. With increasing SiOSi angle, the lengths of the SiO bonded interactions comprising the angle monotonically decrease in a nonlinear fashion, as observed in earlier studies (cf. Gibbs 1982).

All calculations of the ELF were performed with the VASP periodic density functional code (Kresse and Hafner 1993, 1994; Kresse and Furthmüller 1996a,b) using ultrasoft pseudopotentials (Vanderbilt 1990) and the local density approximation to account for the exchange-correlation contribution to the total energy. For the disilicate and cyclosiloxane molecules, single k point ( $\Gamma$  point) calculations were made using the geometry-optimized atomic coordinates obtained with GAUSSIAN98. The molecules were placed in unit cells large enough to prevent interactions between the molecules in adjacent cells. For the bulk crystals coesite, quartz, and stishovite, the unit-cell dimensions and the atomic coordinate were geometry-optimized with VASP using a k-point mesh density (Monkhorst and Pack 1976) sufficient to ensure convergence of the geometry-optimized structure and energy. The ELF and the total valence electron-density distribution isosurface maps, generated with the VASP calculations, were created with the desktop 3-D visualization software of Teriberby et al. (2002). The Laplacian maps were constructed from the wave functions generated with GAUSSIAN98 and the software XTREM and GRID kindly supplied by Richard Bader. The deformation maps were generated from the wave functions with the software DEFORM written by Monte Boisen, Jr.

### ELF maps for disilicate and cyclosiloxane molecules

ELF isosurface maps for the disilicate molecules

The ELF values for the local maxima of the nonbonding region on the bridging oxide anions for each disilicate molecule are given in Table 1 as a function of the SiOSi

**Table 1** SiOSi angles, values of the local maxima of the ELF and 98 percentile values for the non-bonding region of the bridging oxide anions for the  $\text{H}_6\text{Si}_2\text{O}_7$  molecule

SiOSi angle	Maximum ELF	98th percentile
$110^\circ$	0.881	0.863
$120^\circ$	0.878	0.860
$130^\circ$	0.874	0.856
$140^\circ$	0.869	0.852
$150^\circ$	0.863	0.846
$160^\circ$	0.854	0.837
$170^\circ$	0.845	0.828
$180^\circ$	0.835	0.818

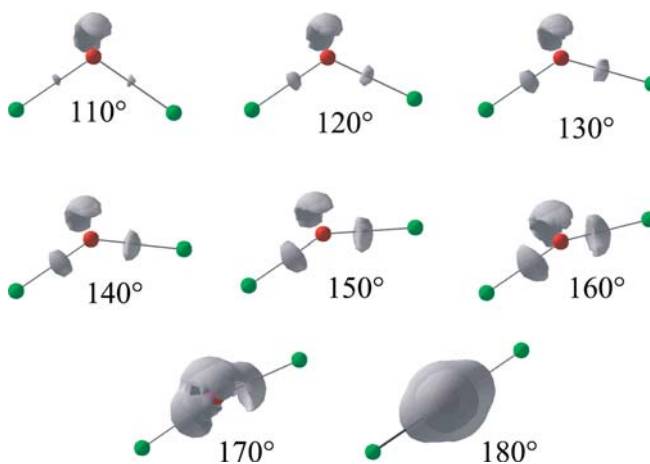


**Fig. 1** 98th percentile ELF isosurfaces generated for the nonbonding regions on the bridging oxide anion calculated for geometry optimized  $\text{H}_6\text{Si}_2\text{O}_7$  molecules with their SiOSi angles fixed at  $110^\circ, 120^\circ, \dots, 180^\circ$ . The red spheres represent O and the green represent Si. As the SiOSi angle widens, the local maxima of the banana-shaped isosurfaces on the bridging oxide anion decreases in value (Fig. 2) as they progressively wrap around the bridging oxide anion until about  $170^\circ$  where the bonding and nonbonding isosurfaces merge. At  $180^\circ$ , the bonding isosurfaces completely envelope a smaller, nearly spherical region of nonbonding regions

angle. The ELF isosurface maps generated for the bridging SiOSi bonded interactions at the 98th percentile for the ELF distribution for the nonbonding region on the bridging oxide anions are displayed in Fig. 1. With increasing SiOSi angle, Fig. 2 shows that the value of the local maxima of the ELF in the nonbonding region decreases from 0.881 to 0.835 as the SiOSi angle increases from  $110^\circ$  to  $180^\circ$  with a small discontinuity at  $\sim 150^\circ$  (see Table 1). Concomitant with the increase in the angle, the 98th percentile banana-shaped isosurface becomes more extended around the anion as the function in the nonbonding region becomes larger (Fig. 1). At  $170^\circ$ , the ELF isosurfaces of the two bonding regions merge with the nonbonding banana-shaped isosurface, and at  $180^\circ$ , the bonding isosurface completely envelops the nonbonding isosurface, which is displayed as a small roughly spherical isosurface at the center of the bonding isosurface. When the ELF value is increased further, the spherical nonbonding isosurface transforms into a thin ring-shaped isosurface around the anion that

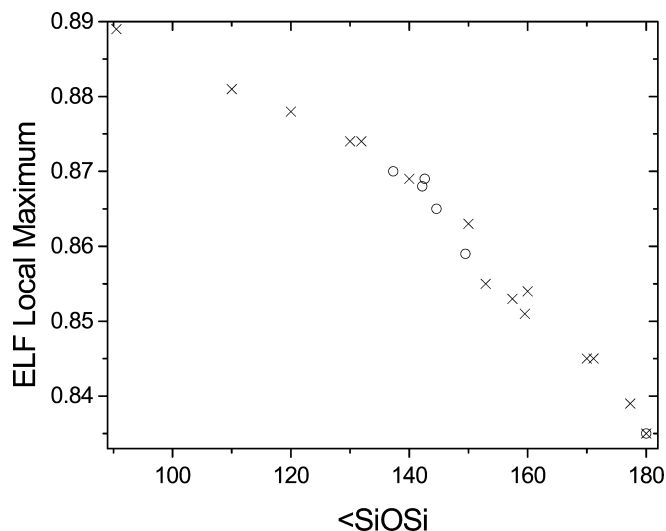


**Fig. 2** A scatter diagram of the ELF local maxima for the nonbonding region on a given oxide anion plotted against the SiOSi angle involving the anion. The data for the disilicate and cyclosiloxane molecules are plotted as crosses and for coesite and quartz are plotted as open circles

breaks up into four very thin plates and then disappears at the local maximum. Unlike the range of values exhibited by the local maxima for the bridging anions, the value exhibited for the nonbonding regions of the nonbridging O atoms remains unchanged at 0.88 as the SiOSi angle increases from 110° to 180°. Likewise, the isosurfaces on the nonbridging anions remain essentially unchanged. The invariance of the isosurfaces and the local maximum with increasing SiOSi angle appears to depend primarily on the invariance of the SiOH angle, which shows little or no change (between 119.2° and 119.8°) as the SiOSi angle increases in value from 110° to 180°. On the other hand, those in the nonbonding regions on each of these anions were found to be reducible. The isosurface on bridging anions for the molecules with a 110° and 120° SiOSi angles were also found to be reducible, while those on the remaining molecules with angles between 130° and 170° were found to be irreducible. The maximum local ELF values (0.882) for the nonbonding regions on the nonbridging oxide anions involving SiOH angles of ~120° are virtually the same as that observed (0.879) for the oxide anion involved in the 120° SiOSi angle.

Given the connection between the ELF value of the local maximum for a nonbonding region and the SiOSi angle, the accuracy with which the position of a proton-docking site can be deduced is expected to be the greatest, all other things being equal, when the nonbonding region involves an oxide anion that comprises a narrow SiOSi angle and the region is well developed. Moreover, the accuracy of the determination is expected to decrease systematically as the angle widens and the ELF isosurface in the nonbonding region becomes more elongated and less localized and the local maximum decreases in value. When the angle is straight, the

banana-shaped nonbonding isosurface is missing and the ELF isosurface is radially distributed around the anion. In short, the favorability of a nonbonding region as a docking site is expected to be larger when the SiOSi angle is narrow and to decrease with increasing angle. For narrow angles, the ELF distribution is more localized, as indicated by the 98th percentile isosurface and its maximum ELF value. As observed above, there is a small discontinuity in the trend of the data in Fig. 2 in the vicinity of 150°, where the decrease in the maximum ELF value with angle increases by a factor of 2. This suggests that oxide anions involved in angles of ~150° and wider can be expected to be unfavorable docking sites relative to those involved in narrower angles. Accordingly, protons can be expected to prefer anions involved in angles less than ~150° in preference to those involved in wide angles given that the nonbonding regions for anions involved in wide angles are radially distributed and reduced in value with appreciably smaller local maxima, while those involved in narrow angles are more localized and well developed with larger local maxima.

#### ELF isosurface maps for the cyclosiloxane molecules

The 98th percentile ELF isosurface maps generated for the cyclosiloxane molecules are displayed in Fig. 3, where it is seen that the shapes of the nonbonding regions about the bridging oxide anions are similar to those generated for the disilicate molecule. The SiOSi angles exhibited by the cyclosiloxane molecules increase with increasing ring size from 90.5° for the cyclo-disiloxane molecule to 131.9° for the cyclotrisiloxane molecule to 157.4° for the cyclotetrasiloxane molecule to 177.3° for the cyclopentasiloxane molecule, and then decrease with further increase in ring size to 171.1° for the cyclohexasiloxane molecule to 159.5° for the cycloheptasiloxane molecule to 152.9° for the cyclo-octasiloxane molecules. The local maximum ELF values for the nonbonding regions are given in Table 2 together with the 98th percentile values. The local maximum values are plotted in Fig. 2 with the disilicate data. As observed for the disilicate molecule, the banana-shaped isosurfaces displayed by the ELF isosurface maps become more elongated about the bridging anion with increasing SiOSi angle. At an angle of 177.3°, the nonbonding isosurface is nearly hemispherical in shape and merged with the bonding isosurfaces, as observed for the disilicate molecule with the straight SiOSi angle. It is noteworthy that the smaller rings differ from the larger ones in one important way. In the case of the cyclo-disiloxane, the cyclotrisiloxane, and cyclotetrasiloxane molecules, the apices of the SiOSi angles extend toward the exterior of each ring whereas for larger rings, the apices extend into the interior (see Fig. 3). These results suggest that for structures with cyclotrisiloxane and cyclotetrasiloxane rings the nonbonding regions will be located outside the rings,

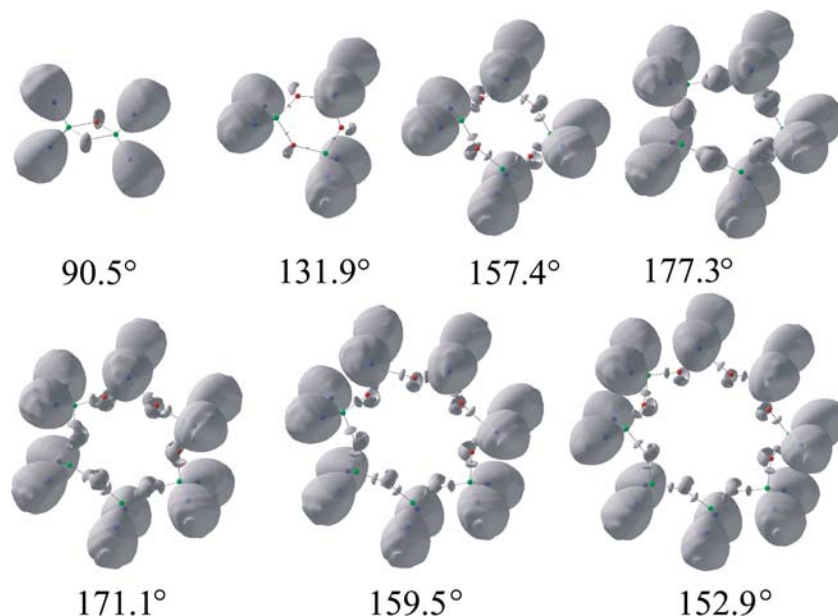


**Fig. 3** 98th percentile ELF isosurfaces generated for the nonbonding regions on the bridging oxide anion calculated for geometry-optimized cyclosiloxane ( $\text{SiOH}_2$ ) $_n$  molecules for  $n = 2$  to 8). The *red spheres* represent O and the *green* ones represent Si. The nonbonding isosurfaces on the bridging oxide anions are similar to those calculated for the the  $\text{H}_6\text{Si}_2\text{O}_7$  molecule. Inasmuch as the H atoms of the molecules lack core attractors, they are accordingly each enclosed by a large teardrop-shaped isosurface (see Savin et al. 1997). Note that the bonding isosurfaces are absent for the cyclodisiloxane molecule, that they are small but present for the cyclotrisiloxane molecule, and that they increase in size with increasing angle

whereas for those with cyclohexasiloxane and larger rings the regions will be located inside the rings. However, for cyclopentasiloxane rings with wide angles, as in melanophlogite, brewsterite, and ZSM-5, for example, the nonbonding regions should be largely spherical in shape. The nonbonding features observed for the cyclohexasiloxane, cycloheptasiloxane, and cyclooctasiloxane molecules are all reducible. The nonbonding regions on the remaining cyclosiloxane molecules are irreducible, with their nonbonding features disappearing at the same ELF value as a single unit. It is notable that the shapes of the nonbonding features and the values of the local maxima (Table 2) for the cyclotrisiloxane, the cyclohexasiloxane, and the cycloheptasiloxane molecules are virtually identical with those of the disilicate molecules with SiOSi angles of  $130^\circ$ ,  $170^\circ$ , and  $160^\circ$ . As observed for the  $\text{H}_6\text{Si}_2\text{O}_7$  molecule, teardrop-shaped isosurfaces are displayed along each SiO bond vector. Likewise, the deformation map for a cyclotetrasiloxane molecule likewise displays maxima along the SiO bond vectors and in the nonbonding region as observed for the disilicate molecule (see also Geisinger et al. 1987). It is noteworthy that the bonding isosurfaces for the cyclodisiloxane molecule are absent along the line between Si and O, suggesting that the structure is weakly bonded together relative to other cyclosiloxane molecules. Silica W is the only known silica polymorph to contain cyclodisiloxane rings. To our knowledge, it has never been reported in

nature, an observation that possibly reflects a weaker SiO-bonded interaction for the ring structure. Collectively, for the cyclosiloxane molecules, as the SiOSi angle widens, the nonbonding feature on the bridging oxide anion becomes progressively more elongated and spherical in shape with decreasing local maxima, as observed for the disilicate molecules, again demonstrating that the bridging oxide anions becomes less favorable as a proton-docking site at wide angles. Given that there is no direct connection between the electron localization function and the electron-density distribution,  $\rho$ ,  $\Delta\rho$  and  $-\nabla^2\rho$  maps were constructed for several disilicate molecules to explore the extent to which the isosurfaces and maxima displayed by these maps correspond with those displayed by the ELF maps.

### A comparison of deformation, valence, Laplacian and ELF maps

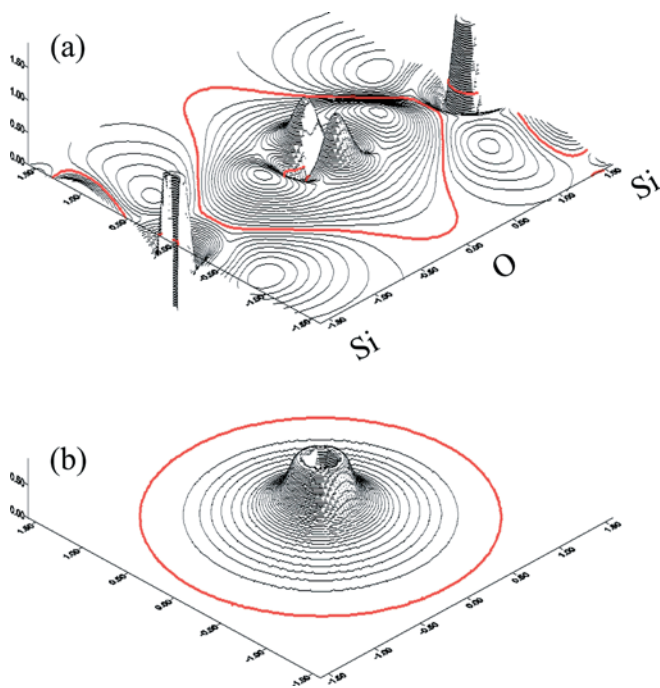
Deformation electron density  $\Delta\rho$  maps

Figure 4 displays a deformation map, calculated for planes through the bridging oxide anion of the  $\text{H}_6\text{Si}_2\text{O}_7$

**Table 2** SiOSi angles, maximum ELF, values and 98 percentiles for the nonbonding region of the bridging oxide anions of of the  $(\text{H}_2\text{SiO})_n$ -cyclosiloxane molecules

Cyclosiloxane	$\angle\text{SiOSi}$	Maximum ELF	98 percentile
$\text{H}_4\text{Si}_2\text{O}_2$	$90.5^\circ$	0.889	0.871
$\text{H}_6\text{Si}_3\text{O}_3$	$131.9^\circ$	0.874	0.856
$\text{H}_8\text{Si}_4\text{O}_4$	$157.4^\circ$	0.853	0.836
$\text{H}_{10}\text{Si}_5\text{O}_5$	$177.3^\circ$	0.839	0.822
$\text{H}_{12}\text{Si}_6\text{O}_6$	$171.1^\circ$	0.845	0.828
$\text{H}_{14}\text{Si}_7\text{O}_7$	$159.5^\circ$	0.851	0.834
$\text{H}_{16}\text{Si}_8\text{O}_8$	$152.9^\circ$	0.855	0.838





**Fig. 4a,b** Deformation electron density distributions,  $\Delta\rho$ , calculated through the bridging oxide anion for the  $\text{H}_6\text{Si}_2\text{O}_7$  molecule with a  $180^\circ$  angle in planes parallel (a) and perpendicular (b) to the SiOSi line. In a, the level line contours (isosurfaces) of the bonding electron density completely envelops the nonbonding electron density as observed for the  $180^\circ$  configuration in Fig. 1. The electron density of the nonbonding electron density in b is seen to be delocalized in a spherical distribution around the SiOSi line. The combined maps reveal that the deformation electron-density distribution forms a spherical ring-shaped isosurface of electron density around the oxide anion rather than a spherical isosurface of electron density. The value of the electron-density distribution is given by the vertical scale at the upper left of each figure. The zero contour level is displayed as a red solid line

molecule with the  $180^\circ$  angle, along and perpendicular to the SiOSi line. The maps display isosurfaces that are similar to the isosurfaces displayed by the ELF isosurface maps generated for the molecule (Fig. 1). Figure 4a shows that the  $\Delta\rho$  zero level line isosurface of the bonding electron distribution encloses the isosurfaces of the nonbonding electron distribution while Fig. 4b shows that the isosurfaces of the nonbonding distribution are radially distributed in a ring of electron density around the oxide anion, a distribution similar to that displayed by the ELF. Further, previous mappings of the deformation electron-density distributions for the SiOSi bonded interactions for several  $\text{H}_6\text{Si}_2\text{O}$  and  $\text{H}_6\text{Si}_2\text{O}_7$  molecules and for coesite (Geisinger et al. 1987; Downs 1995, Gibbs et al. 2002) display a pattern of isosurfaces and maxima about the bridging anion that is strikingly similar to that displayed by the ELF maps.

#### Total valence electron density $\rho$ isosurface maps

Valence maps for the  $\text{H}_6\text{Si}_2\text{O}_7$  molecules display features around the oxide anions that are likewise similar to

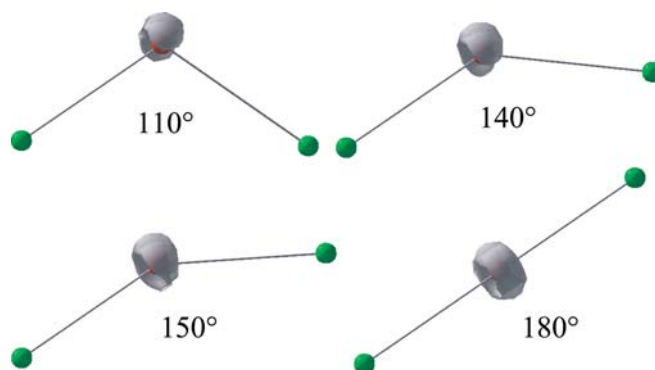


**Fig. 5** Total valence electron density  $6.8e^{-3} \text{ \AA}^{-3}$  isosurface maps for the SiOSi bonded interactions comprising selected disilicate molecules. The green spheres represent Si and the red represent O. Note that as the SiOSi angle widens, the banana-shaped isosurfaces increase in their extension around the oxide anions with two ends merging in a ring-shaped isosurface at  $180^\circ$ . Also, the local maximum of the isosurfaces decreases from  $7.53e^{-3} \text{ \AA}^{-3}$  at  $110^\circ$  to  $7.09e^{-3} \text{ \AA}^{-3}$  at  $180^\circ$

those displayed by ELF and  $\Delta\rho$  distributions. The distributions are similar (Fig. 5) in that they exhibit banana-shaped  $\rho$  isosurfaces in the nonbonding region when the SiOSi angle is bent. Further, as the SiOSi angle widens, the banana-shaped  $\rho$  isosurface increases in its extent around the bridging anion and becomes radially distributed as a ring-shaped isosurface, as observed in the last section. Also, the maximum  $\rho$  value for the isosurface decreases progressively with increasing SiOSi angle from  $7.53e^{-3} \text{ \AA}^{-3}$  at  $110^\circ$  to  $7.28e^{-3} \text{ \AA}^{-3}$  at  $130^\circ$  to  $7.23e^{-3} \text{ \AA}^{-3}$  at  $150^\circ$  to  $7.14e^{-3} \text{ \AA}^{-3}$  at  $170^\circ$  to  $7.09e^{-3} \text{ \AA}^{-3}$  at  $180^\circ$ , reflecting the progressive delocalization of the valence electron density into a thin ring-shaped isosurface around the anion as the angle widens. The decrease in the maximum  $\rho$  value with increasing angle corresponds to the decrease in the maximum value of the nonbonding regions displayed by the ELF. At least in the case of SiOSi-bonded interactions, the features in the deformation and total valence maps are consistent with the way the maxima and the shape of the isosurface for the nonbonded regions change with angle. Although the total valence isosurface maps fail to display maxima along the SiO bond, a mapping of the electron density along the SiO bond vectors display maxima  $6.45e^{-3} \text{ \AA}^{-3}$  and  $6.43e^{-3} \text{ \AA}^{-3}$  in height along the vectors for molecules with  $140^\circ$  and  $180^\circ$  angles, respectively. The bonding and nonbonding maxima displayed by the maps are located  $\sim 0.35 \text{ \AA}$ , on average, from the bridging oxide anion.

#### Scalar Laplacian $-\nabla^2\rho$ maps

As observed by Bader et al. (1984), MacDougall (1984), Bader and MacDougall (1985) and Bader et al. (1996), the local maxima displayed by  $-\nabla^2\rho$  maps define regions where the bonding and nonbonding electron density distribution is locally concentrated. To examine the extent to which these maxima correspond

with the maxima displayed in the ELF maps,  $-\nabla^2\rho$  maps were generated for the  $\text{H}_6\text{Si}_2\text{O}_7$  molecules with SiOSi angles of  $120^\circ$ ,  $140^\circ$ ,  $160^\circ$ , and  $180^\circ$ . Two maps were constructed for each molecule, one for the plane containing the angle and the other for the perpendicular plane that bisects the angle (Fig. 6a,b, respectively). The maps for the  $120^\circ$  and  $140^\circ$  molecules each show crescent-shaped isosurfaces ascribed to a region of bonding electrons along the SiO bond vectors at a distance of  $0.37 \text{ \AA}$  from the bridging oxide anion (Fig. 6a) and larger crescent-shaped isosurfaces in the lone-pair region at a distance of  $0.35 \text{ \AA}$  (Fig. 6b). The latter isosurface extends about three quarters of the way about the anion. The isosurfaces along each SiO bond vector for the  $140^\circ$  molecule are more elongated than those exhibited by the  $120^\circ$  molecule. Also, the isosurfaces in the nonbonding region extend almost completely about the anion. For the  $160^\circ$  molecule, the nonbonding isosurfaces are merged with the bonding isosurface to form a single isosurface that encloses much of the anion, whereas for the  $180^\circ$  angle molecule, the isosurface completely surrounds the anion. Thus, with increasing SiOSi angle, the electron density in the bonding and nonbonding regions become progressively locally

concentrated and the two regions merging to form a quasishaped sphere of locally concentrated electron density about the anion at  $180^\circ$ . It is noteworthy that maps constructed for the O1 anion involved in the  $170^\circ$  SiOSi angle in beryl (Prencipe 2002) display a similar distribution of locally concentrated isosurfaces of electron density. The nonbonding and bonding isosurfaces are merged to form isosurfaces of locally concentrated electron density that completely envelope the anion. However, the observation that the electron density is locally concentrated in a sphere about the anion cannot be used to assert that there is a spherical buildup of electron density about the anion.

A location of the  $(3,-3)$  critical points in the  $-\nabla^2\rho$  distribution about the bridging anion for the  $120^\circ$  molecule with the software BUBBLE shows two maxima in the nonbonding region, each at a distance of  $0.368 \text{ \AA}$  from the anion, and six maxima about the anion for the  $180^\circ$  molecule at a distance of  $0.355$  from the anion. Two  $(3,-3)$  critical points were found in the bonding region and one in the region for the nonbonding regions for the  $140^\circ$  molecule and one in the nonbonding region of the  $160^\circ$  molecule. Because of the spacing of the contours, the  $-\nabla^2\rho$  maps displayed in Fig. 6 do not show two peaks in the nonbonding region for the  $160^\circ$  molecule and six for the  $180^\circ$  molecule. It is clear that the isosurfaces and the local maxima displayed by the valence, deformation, and Laplacian maps are in close correspondence with those displayed by the ELF maps. As such, the correspondence provides a physical basis for considering the ELF function as a measure of the localization of the electron density in regions ascribed to bonding and nonbonding electrons (cf. Bader et al. 1996).

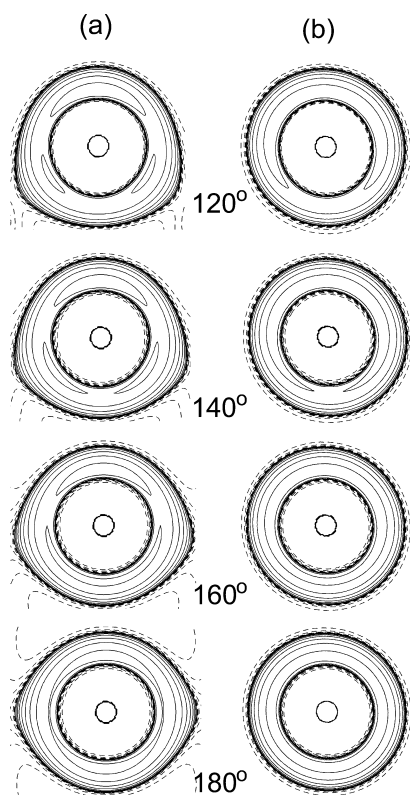


**Fig. 6** Laplacian  $-\nabla^2\rho$  maps calculated for the bridging oxide anion of the  $\text{H}_6\text{Si}_2\text{O}_7$  molecule in the plane of the SiOSi angle (column **a**) and in the perpendicular plane bisecting the SiOSi angle (column **b**). The contour interval is  $0.0, \pm 0.002, \pm 0.004, \pm 0.008e \text{ \AA}^{-5} \dots$ , the positive contours are drawn as *solid lines*, the negative as *dashed lines* and the zero level contour as *alternating short and long dashed lines*. The cutoff was set at  $\pm 150e \text{ \AA}^{-5}$

### Docking sites for hydrogen atoms in the silica polymorphs

Favorable docking sites for hydrogen in coesite

As observed above, a study of the FTIR spectra recorded for several protonated coesite crystals (Koch-Müller et al. 2001) shows that the hydrogen atoms in the structure avoid O1 and protonate O2, O3, O4, and O5. The O1 anion is involved in a  $180^\circ$  SiOSi angle whereas the remaining four anions are involved in narrower angles that range in value between  $137.6^\circ$  and  $149.7^\circ$ . This observation indicates, as observed for the disilicate and cyclosiloxane molecules, that the size of the angle plays a pivotal role in governing the extent to which the nonbonding region is developed as a banana-shaped ELF isosurface on the bridging oxide anion. With the exception of the position of the H2B atom, which was found to protonate O4, the positions of the hydrogen atoms determined in the FTIR study are in reasonably good agreement with the positions of the local maxima of the nonbonding isosurfaces (see Koch-Müller et al. 2001) for the nomenclature used for the hydrogen atoms in the

protonated coesite crystal. The ELF isosurfaces generated for the SiOSi bonded interactions in coesite are displayed in Fig. 7. The 98th percentile isosurfaces are similar to those generated for the disilicate and cyclo-siloxane molecules. In fact, the values of the local maxima for the isosurfaces for the nonbonding regions on the oxide anions in coesite are virtually identical with those generated for the molecules (Figs. 1–3). The distances between the hydrogen atoms determined in the FTIR study and the positions of the local maxima (denoted lm) for the nonbonding isosurfaces on O2, O3, O4, and O5 are 0.62, 0.61, 1.24, and 0.44 Å, respectively. Further, the SiOH angles determined in the FTIR study at O2, O3, O4, and O5 are 100.5°, 127.5°, 101.0.7°, and 91.5°, respectively, compared with the SiOlm angles at these anions of 109.0°, 106.5°, 103.3°, and 111.4°, respectively.

Given the positions of the oxide anions that comprise the  $\nu(\text{OH})_4$  group and those for the local maxima of the banana-shaped isosurfaces, the position of each model H atom was found by stepping away from the oxide anion along the line connecting the anion and the position of the local maxima at a distance of 0.96 Å. For the sake of convenience, the model hydrogen atoms located in this fashion were denoted as h. This results in an Oh distance of 0.96 Å, the geometry-optimized OH bond length obtained for the  $\text{H}_6\text{Si}_2\text{O}_7$  molecules. The positional coordinates for the four model atoms determined with the stepping strategy are given in Table 3. The distances between the nearest neighbor Si and H

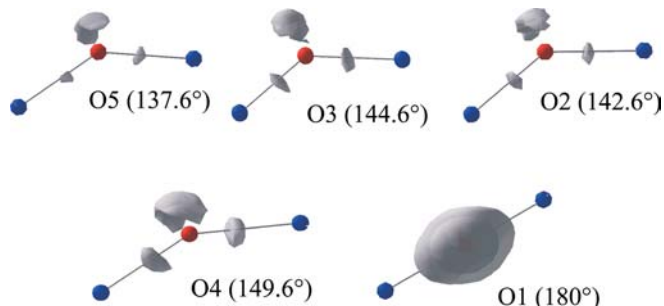


**Fig. 7** 98th percentile ELF isosurfaces generated for the nonbonding region on the bridging oxide anions comprising the SiOSi-bonded interactions in coesite. The red spheres represent O and the blue ones represent Si

**Table 3** Coordinates of the local maxima, lm, for regions of nonbonding electrons and docking sites for the model hydrogen atoms, h, in coesite

Local maxima, lm	x	y	z
lm2	0.500	0.072	0.750
lm3	0.800	0.123	0.649
lm4	0.315	0.063	0.345
lm5	0.403	0.300	0.523
h2	0.500	0.038	0.750
h3	0.845	0.122	0.712
h4	0.317	0.028	0.361
h5	0.351	0.308	0.522

atoms of the  $\nu(\text{OH})_4$  group found by Koch–Müller et al. (2001) range between 1.875 and 2.390 Å, whereas those between the nearest-neighbor Si atoms and the positions of the model hydrogen atoms show a similar but smaller range of values between 2.057 and 2.166 Å. A drawing of the coesite structure displaying the group is given in Fig. 8 viewed down  $[-1 -1 8]$ . The angles between the OH vectors determined in this study are  $\angle \text{h2-O2-H1} = 45.8^\circ$ ,  $\angle \text{h3-O3-H3} = 29.1^\circ$ ,  $\angle \text{h4-O4-H2B} = 110.1^\circ$ , and  $\angle \text{h5-O5-H2A} = 23.8^\circ$ . The agreement is best for the angle involving the O5 oxide anion and poorest for the angle involving the O4 oxide anion. It was observed earlier that the accuracy with which the position of a proton can be determined is expected to depend on the size of the SiOSi angle with the most accurate determination being made for an oxide anion involved in a narrow SiOSi angles. The  $\angle \text{Si1-O5-Si2}$  is the narrowest angle in coesite ( $136.7^\circ$ ) and, as expected, shows the best agreement with an  $\text{h5-O5-H2A}$  angle of  $23.8^\circ$ . The  $\text{Si1-O4-Si2}$  angle is the widest angle ( $149.7^\circ$ ), involving the four oxide anions of the  $\nu(\text{OH})_4$  group. In this case, the agreement is the poorest, as expected, with an  $\text{h4-O4-H2B}$  angle of  $110.1^\circ$ . The remaining two angles,  $\text{h2-O2-H1} = 45.8^\circ$  and  $\text{h3-O3-H3} = 29.1^\circ$ , although intermediate values, are relatively small. Note that the banana-shaped  $\rho$  isosurface starts to merge with the bonding isosurfaces at  $\sim 150^\circ$  (Fig. 5). On the basis of these results, it appears that the strategy used in this study can be used to generate Oh bond vectors that agree reasonably well with those observed, particularly when the SiOSi angle is relatively narrow. Given the

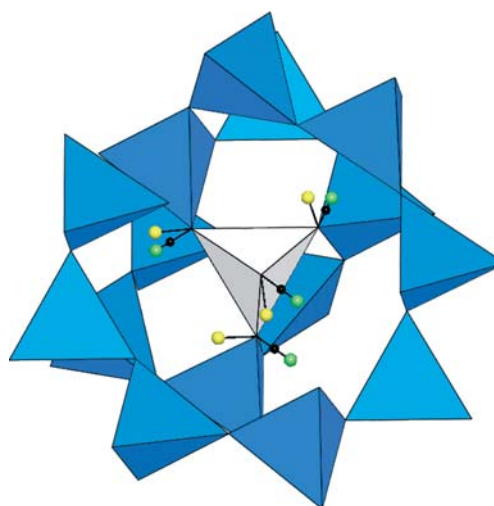


**Fig. 8** A polyhedral drawing of a block of the coesite structure viewed down  $[-1 -1 8]$ . The sky blue tetrahedra represent  $\text{SiO}_4$  silicate tetrahedra and the white one represents the defect  $(\text{OH})_4$  group. The small yellow spheres denote the positions of H atoms determined by Koch–Müller et al. (2001), the black spheres denote the positions of the local maxima of the nonbonding regions on the oxide anions, and the light green spheres denote the positions of the model hydrogen h atoms determined in this study. Each model hydrogen was located 0.95 Å from an oxide anion



relaxation of the atoms that must take place in a structure when a  $v(\text{OH})_4$  group is formed together with the nonbonded repulsions that obtain between the H and Si atoms, it is surprising that the observed and model positions of the H atoms in coesite agree as well as they do.

#### $\rho$ isosurface maps for coesite

Total valence electron-density distribution maps were also generated for the five nonequivalent SiOSi bonded interactions in coesite (Fig. 9). As the SiOSi angle widens from  $136.7^\circ$  to  $180.0^\circ$ , the maximum value of  $\rho$  decreases from  $7.20e \text{ \AA}^{-3}$  to  $7.06e \text{ \AA}^{-3}$ . The maximum value for the  $180.0^\circ$  angle is  $0.03e \text{ \AA}^{-3}$  smaller than that obtained for the  $\text{H}_6\text{Si}_2\text{O}_7$  molecule while that for the  $149.6^\circ$  angle ( $7.21e \text{ \AA}^{-3}$ ) in coesite is  $0.02e \text{ \AA}^{-3}$  less than that obtained for the molecule with a  $150^\circ$  angle. Clearly, the maximum values of the valence electron-density distributions for coesite and the  $\text{H}_6\text{Si}_2\text{O}_7$  are in close agreement. The valence electron-density distribution is banana-shaped for the four anions involved in the narrowest angles in coesite while it is a circular ring-shaped isosurface when the angle is  $180^\circ$ , as observed for the  $\text{H}_6\text{Si}_2\text{O}_7$  molecule. The features displayed by the ELF,  $\Delta\rho$  and  $\rho$ , and  $-\nabla^2\rho$  distributions in the nonbonding regions of the four molecules and the crystals are strikingly similar despite the smaller number of atoms in the molecules. Collectively, these results suggest that electron density in coesite is highly localized in the vicinity of the nonbonded regions of  $\text{O}_2$ ,  $\text{O}_3$ , and  $\text{O}_5$ , less so in the vicinity of  $\text{O}_4$ , and much less so in the vicinity of  $\text{O}_1$ .

#### Favorable docking sites for protons in stishovite:

The structure of the high-pressure silica polymorph stishovite consists of corner- and edge-sharing silicate octahedra such that each Si cation is coordinated by six oxide anions and each oxide anion is coordinated by three Si cations. The ELF isosurface map generated for the polymorph at the 98th percentile viewed down  $[001]$

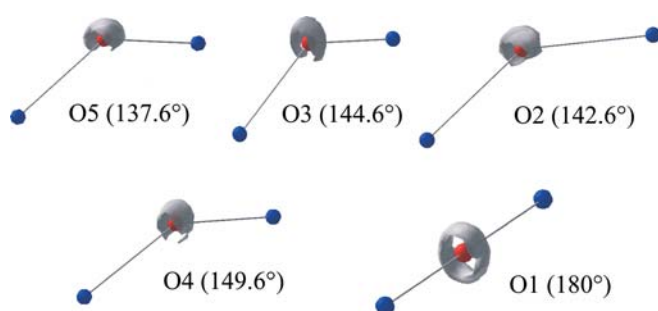


**Fig. 9** Total valence electron density  $6.8e \text{ \AA}^{-3}$  isosurface maps for the nonequivalent SiOSi bonded interactions in coesite. The blue spheres represent Si and the red represent O. Note that as the SiOSi angle widens, the banana-shaped isosurfaces increase in their extension around the oxide anions

(Fig. 10) shows that each oxide anion in the structure is also coordinated by five teardrop-shaped isosurfaces, three located along the three SiO vectors that reach each anion, one located next to the anion on one side of the plane defined by the three vectors and the other located next to the anion on the other side of the plane. The distribution of these isosurfaces was found to be in an one-to-one correspondence with the five maxima recorded around the anion in experimental deformation maps (Spackman et al. 1987; Gibbs et al. 2001; Kirfel et al. 2001). It has been postulated that protons substitute in the stishovite structure in the same way that they do in the rutile  $\text{TiO}_2$  structure with the OH bond vector oriented perpendicular to  $[001]$  (Rossman and Smyth 1990). After confirming that the OH bond vector is oriented perpendicular to  $[001]$ , Pawley et al. (1993) postulated that the proton is docked “just off the shared OO edge” of the silicate octahedra. On the basis of the position of local maxima of the nonbonding isosurface in stishovite and using the same strategy used to find the position of the protons in coesite, the most favorable docking site for the model hydrogen atom was found to be at 0.12, 0.44, 0.00. This places the model hydrogen off the shared OO edge of the octahedra at a distance of  $0.96 \text{ \AA}$  from one of the oxide anions (Fig. 11) such that the Oh vector is oriented  $92.5^\circ$  to  $[001]$  (Ross et al. (Accepted)).

#### Favorable docking sites for protons in quartz

As observed above, each oxide anion in quartz is coordinated by a nonbonding banana-shaped isosurface and two bonding teardrop isosurfaces (Gibbs et al. 2001, 2002). A map of the 98th percentile isosurface for the nonbonding regions for a silicate tetrahedron is

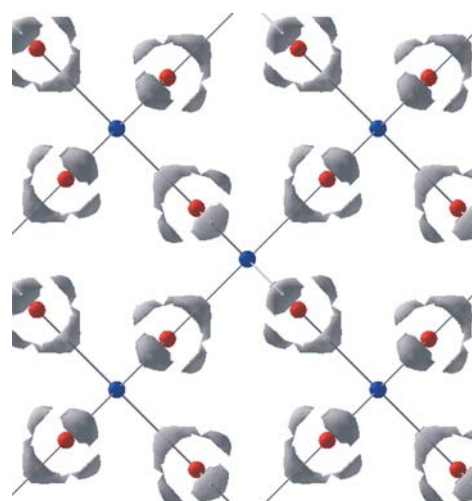


**Fig. 10** 98th percentile ELF-isosurfaces generated for stishovite viewed down  $[001]$ . The red spheres represent O and the blue ones Si. The bonding electron envelopes lie along the SiO vectors and the nonbonding isosurface lie off the vectors

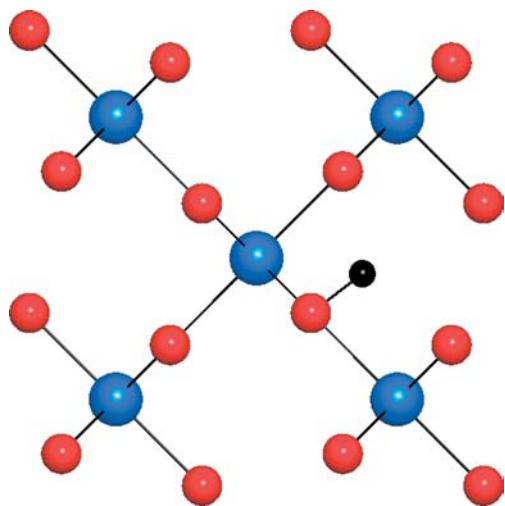


**Fig. 11** A drawing of the structure of stishovite viewed down [001]. The large blue spheres represent Si, the intermediate red ones represent O and the small blue sphere represents the model hydrogen

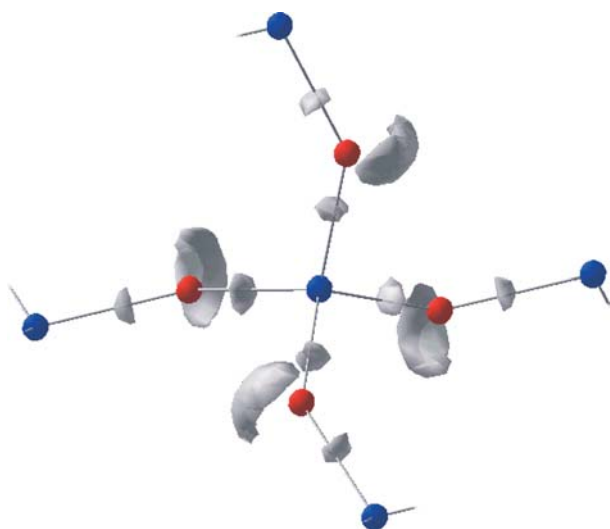


**Fig. 12** 98th percentile isosurfaces calculated for the bonding and nonbonding regions of a silicate tetrahedron in quartz. The red spheres represent O and the black ones represent Si

displayed in Fig. 12. As observed for coesite, the features of the maps are similar to those displayed for the molecules. Also, the local maximum value for the nonbonding region matches those obtained for the molecules and for coesite (Fig. 2). According to Rossman and Smyth (1990) and Mosenfelder (1997), natural coesite observed to date tends to be hydrogen-free. However, synthesis experiments, not only by Koch-Müller (2001) but also by Li et al. (1997) and Mosenfelder (2000), show that synthetic coesite can accommodate H in small amounts ( $\sim 1300$  ppm) in the form of  $v(\text{OH})_4$  groups at high pressures and temperatures. However, the absence of H in natural coesite has led to the speculation that it can accommodate such groups at the pressure and temperature conditions deep in the Earth, but upon

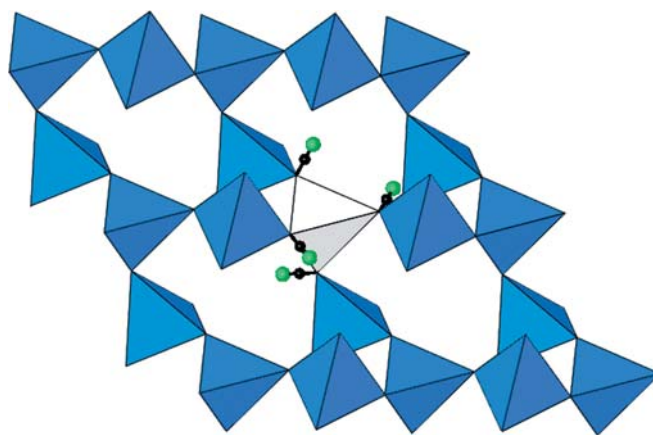


**Fig. 13** A polyhedral drawing of a model  $v(\text{OH})_4$  defect group in quartz viewed about  $10^\circ$  off [001]. The white tetrahedron represents the vacant  $v$  tetrahedron centered at 0.534, 0.534, 0.500, and the black spheres represent the model protons whose positions are given by the orbit  $x, y, z; 1-x, 1-x+y, \frac{2}{3}-z; y, x, 1-z; 1-x+y, 1-x, z + \frac{1}{3}$  where  $x = 0.248, y = 0.281, z = 0.192$

exhumation it undergoes a back reaction and transforms to quartz (Mosenfelder and Bohlen 1997; Zinn et al. 1997). In such a case, the quartz product may possibly contain some relic  $v(\text{OH})_4$  groups. However, to our knowledge, such specimens have yet to be described.

If relic  $v(\text{OH})_4$  groups exist, then the strategy used to locate the hydrogen atoms in coesite can be used to predict the positions of the atoms in quartz. The favorable positions for the model h atoms of the group are given in the legend to Fig. 13. The distances between the h atoms and the next-nearest Si atoms (2.136 and 2.143 Å) are also similar to those observed for coesite. In reasonable agreement with the angles observed for protonated coesite (Koch-Müller et al. 2001), two of the  $v\text{Oh}$  angles of the group are  $108.4^\circ$  and two are  $109.4^\circ$ . On the basis of infrared vibrational frequencies observed for quartz, Kats (1990) predicted that the angle between the OH bond vector of an  $\text{AlO}_4$  group in quartz and [001] is  $\sim 75^\circ$ ,  $45^\circ$  larger than that predicted ( $\sim 120^\circ$ ) between [001] and the Oh bond vector of the vacant  $v(\text{OH})_4$  group. Again, given the relaxation of the structure accompanying the formation of a  $v(\text{OH})_4$  group, the actual orientations of the OH vectors may depart from those obtained for the group by as much as  $40^\circ$ .

## Observations

The electron-density distribution is the most fundamental property of a material, that not only determines the structure and the ground-state properties but also the sites that are susceptible to nucleophilic and electrophilic attack and proton docking. In this study, it was found that the SiOSi bonded interactions in coesite, as revealed in a mapping of the electron localization function, yields nonbonding regions that reside, in three of four cases, in the vicinity of the protons determined in

an infrared study. In point of fact, the positions of model protons determined on the basis of the maxima of the nonbonding isosurfaces agree, with one exception, to within  $\sim 0.6$  Å, on average, with the FTIR values. It was also found that the favorability of proton-docking sites for silica polymorph like quartz and coesite depends on size of the SiOSi angle; the wider the angle, the less favorable the site. Also, the accuracy in the determination of the position was found to depend on the angle with the accuracy increasing with decreasing angle. In agreement with infrared studies for stishovite, a determination of the docking site placed the proton just off the shared OO edge of the octahedra at a distance of 0.96 Å from one of the oxide anions such that the OH vector is nearly perpendicular to [001]. The agreement of the positions determined for the protons in coesite and stishovite and those observed suggests that the electron localization function can provide important information on the location of favorable proton-docking sites for earth materials. As shown by Ross (Accepted), the positions of the (3, -3) critical points displayed by  $-\nabla^2\rho$  can also be used to locate favorable proton-docking sites for high-pressure silicates. For insight into the mechanism of proton transfer, the reader is referred to an elegant paper by Trout and Parrinello (1999) on the dissociation of H<sub>2</sub>O molecules in water where the protons of the molecules are transferred to the nonbonding isosurface of another molecule to form a H<sub>3</sub>O<sup>+</sup> molecule (see also Fuster and Silvi, 2000).

#### Future work

In our ongoing study of the similarity of the bonded interactions exhibited by the silica polymorphs and representative molecules, we plan to geometry-optimize slabs of the structures of coesite, quartz, and stishovite. Following these calculations, water molecules will be introduced to explore where on the surfaces of the slabs the protons of the molecules dock. The connection between proton docking and the extent to which nonbonding regions on bridging and nonbridging anions are developed will be of interest. We also plan to remove an Si atom by creating a defect site and to introduce four hydrogen atoms into coesite and stishovite slabs to determine the location of the H and the effect of the defect on the local structure. In addition, an Si atom will be replaced by Al and H in the quartz and stishovite structures to determine the location and the orientation of the OH vector and the degree to which the structure relaxes about the defect. Also, the structures of several aluminosilicate materials including the alkali feldspars, selected zeolites, cordierite, and sillimanite will be geometry-optimized. These crystals are of interest not only because they contain SiOAl angles that range between  $\sim 115^\circ$  and  $\sim 180^\circ$ , but also because they provide an opportunity to study the development of the nonbonding regions and the docking of protons on surfaces populated with oxide anions involved in SiOAl-bonded

interactions. Such interactions are of interest in that they are believed to play a central role in governing the acidity and catalytic properties of a zeolite. Finally, we plan to evaluate the bulk moduli of the blocks to explore the effect of the defects on the strength of the materials.

**Acknowledgements** The NSF and DOE are thanked for supporting this study with grants EAR-9627458 (G.V.G and M.B.B) and DE-FG02-97ER14751 (D.F.C), respectively. The early phases of this study were completed in collaboration with R.T.D while G.V.G was a Visiting N.S.F Sponsored Scholar at the University of Arizona. The faculty and the graduate students at that institution are thanked for their kind hospitality and for making the visit a stimulating and very worthwhile experience. George Rossman is thanked for generously sharing with G.V.G his extensive knowledge about H in quartz and stishovite.

#### References

- Bader, RFW (1990) Atoms in molecules. Oxford Science Publications, Oxford, UK
- Bader RFW, MacDougall, PJ (1985) Toward a theory of chemical reactivity based on charge density. *J Am Chem Soc* 107: 6788–6795
- Bader RFW, MacDougall PJ, Lau CDH (1984) Bonded and nonbonded charge concentrations and their relation to molecular geometry and reactivity. *J Am Chem Soc* 106: 1594–1605
- Bader RFW, Johnson S, Tang TH, Popelier PLA (1996) The electron pair. *J Phys Chem* 100: 15398–15415
- Becke AD, Edgecombe KE (1990) A simple measure of electron-localization in atomic and molecular systems. *J Chem Phys* 92: 5397–5403
- Burdett JK, McCormick TA (1998) Electron localization in molecules and solids: the meaning of ELF. *J Phys Chem (A)* 102: 6366–6372
- Downs, JW (1995) The electron density distribution of coesite. *J Phys Chem* 99: 6849–6856
- Fuster F, Silvi B (2000) Determination of protonation sites in bases from topological rules. *Chem Phys* 252: 279–287
- Geisinger KL, Spackman MA, Gibbs GV (1987) Exploration of structure, electron-density distribution and bonding in coesite with Fourier and pseudoatom refinement methods using single-crystal X-ray diffraction data. *J Phys Chem* 91: 3237–3244
- Gibbs GV (1982) Molecules as models for bonding in silicates. *Am Mineral* 67: 421–450
- Gibbs GV, Downs JW, Boisen MB (1994) The elusive SiO bond, SILICA. *Reviews in Mineralogy*, vol. 29, Eds. Heaney PJ, Prewittand CT, Gibbs GV (eds) Chap. 10, American Mineralogist, Washington, DC 331–368
- Gibbs GV, Boisen MB, Rosso KM, Teter DM, Bukowski MST (2000) Model structures and electron density distributions of the silica polymorph coesite at pressure: an assessment of OO-bonded interactions, *J Phys Chem (B)* 104: 10534–10542
- Gibbs GV, Boisen MB, Beverly LL, Rosso KM (2001) A computational quantum chemical study of the bonded interactions in earth materials and structurally and chemically related molecules. *Molecular modeling theory: applications in the geosciences. Reviews in Mineralogy and Geochemistry*, vol. 42. Eds. Cygan RT, Kubicki JD (eds). Rosso JJ (series ed) Mineralogical Society of America, Washington, DC pp. 345–382
- Gibbs GV, Cox DF, Crawford TD, Boisen MB, Lim M (2002) A mapping of the electron localization function for the silica polymorphs: evidence for domains of electron pairs and sites of potential electrophilic attack. *Phys Chem Min* 29: 307–318
- Gillespie RJ (1970) The electron-pair repulsion model for molecular geometry. *J Chem Educ* 47: 18–23
- Kats A (1962) Hydrogen in alpha quartz. *Philips Res Rpts* 17: 133–195; 201–279

- Kirfel A, Krane HG, Blaha P, Schwartz K, Lippmann T (2001) Electron-density distribution in stishovite, SiO<sub>2</sub>: a high energy synchrotron radiation study. *Acta Crystallogr (A)* 57: 663–677
- Koch-Müller M, Fei Y, Hauri E, Liu Z (2001) Location and quantitative analysis of OH in coesite. *Phys Chem Miner* 28: 693–705
- Kresse G, Hafner J (1993) Ab initio molecular dynamics for liquid metals. *Phys Rev (B)* 47: 558–561
- Kresse G, Hafner J (1994) Ab initio molecular-dynamics simulation of the liquid-metal amorphous-semiconductor transition in germanium. *Phys Rev (B)* 49: 14251–14269
- Kresse G, Furthmüller J (1996a) Efficiency of ab-initio total energy calculations for metals and semiconductors using a plane-wave basis set. *Comput Mat Sci* 6: 15–50
- Kresse G, Furthmüller J (1996b) Efficient iterative schemes for ab initio total-energy calculations using a plane-wave basis set. *Phys Rev (B)* 54: 11169–11186
- Lasaga AC (1990) Atomic treatment of mineral–water surface reactions In: Hochella MF Jr, White AF (eds) *Mineral–water interface geochemistry*. Reviews in Mineralogy, vol. 23. Chap 2, American Mineralogist, Washington, DC 17–85
- Lasaga AC, Gibbs GV (1990) Ab initio quantum mechanical calculations of water–rock interactions: adsorption and hydrolysis reactions. *Am J Sci* 290: 263–295
- Lewis GN (1966) *Valence and the structure of atoms and molecules*. Dover Press, New York
- Li W, Lu R, Yang H, Prewitt CT, Fei Y (1997) Hydrogen in synthetic coesite crystals. *EOS* 78: 736
- MacDougall PJ (1989) The Laplacian of the electron charge distribution. PhD Thesis, McMaster University 1–128
- Monkhorst HJ, Pack JD (1976) Special points for Brillouin-zone integrations. *Phys Rev (B)* 13: 5188–5192
- Mosenfelder JL (2000) Pressure dependence of hydroxyl solubility in coesite. *Phys Chem Miner* 27: 610–617
- Mosenfelder JL, Bohlen SR (1997) Kinetics of the coesite to quartz transformation. *Earth Planet Sci Let* 153: 133–147
- Prencipe M (2002) Ab initio Hartree–Fock study and charge density analysis of beryl, (Al<sub>4</sub>Be<sub>6</sub>Si<sub>12</sub>O<sub>36</sub>). *Phys Chem Miner* 29: 552–561
- Raulot JM, Baldinozzi G, Seshadri R (2002) An ab initio study of the role of lone pairs in the structure and insulator–metal transition in SnO and PbO. *Sol State Sci* 4: 467–474
- Ross NL, Gibbs GV, Rosso KM (Accepted) Potential docking sites and positions of hydrogen in high–pressure silicates. *Am Mineral*
- Rossman GR (1996) Studies of OH in nominally anhydrous minerals. *Phys Chem Miner* 23: 299–304
- Rossman GR, Smyth JR (1990) Hydroxyl contents of accessory minerals in mantle eclogites and related rocks. *Am Mineral* 75: 775–780
- Pawley AR, McMillan PF, Holloway JR (1993) Hydrogen in stishovite, with implications for mantle water content. *Science* 261: 1024–1026
- Savin A, Nesper R, Wengert S, Fässler TF (1997) ELF: the electron localization function. *Ang Chem Inter English* (ed) 36: 1808–1832
- Spackman MA, Hill RJ, Gibbs GV (1987) Exploration of structure and bonding in stishovite with Fourier and pseudoatom refinement methods using single-crystal and powder X-ray diffraction data. *Phys Chem Miner* 14: 139–150
- Terriberry TB, Cox DF, Bowman DA (2002) A tool for the interactive 3-D visualization of electronic structures in molecules and solids. *Comput Chem* 26: 313–319
- Trout BL, Parrinello M (1999) Analysis of the dissolution of H<sub>2</sub>O using first–principles molecular dynamics. *J Am Chem Soc (B)* 103: 7340–7345
- Vanderbilt D (1990) Soft self-consistent pseudopotentials in a generalized eigenvalue formalism. *Phys Rev (B)* 41: 7892–7895
- Zinn P, Hinze E, Lauterjung J, Wirth R (1997) Kinetics and microstructural studies of the quartz–coesite phase transition. *Phys Chem Earth* 22: 105–111